

SCIENTIFIC REPORTS



OPEN

Preparation of Carbon Nanotube/ TiO₂ Mesoporous Hybrid Photoanode with Iron Pyrite (FeS₂) Thin Films Counter Electrodes for Dye-Sensitized Solar Cell

Received: 02 March 2016

Accepted: 13 May 2016

Published: 31 May 2016

Bayram Kilic¹, Sunay Turkdogan¹, Aykut Astam², Oguz Can Ozer¹, Mansur Asgin¹,
Hulya Cebeci³, Deniz Urk⁴ & Selin Pravadili Mucur⁵

Multi-walled carbon nanotube (MWCNT)/TiO₂ mesoporous networks can be employed as a new alternative photoanode in dye-sensitized solar cells (DSSCs). By using the MWCNT/TiO₂ mesoporous as photoanodes in DSSC, we demonstrate that the MWCNT/TiO₂ mesoporous photoanode is promising alternative to standard FTO/TiO₂ mesoporous based DSSC due to larger specific surface area and high electrochemical activity. We also show that iron pyrite (FeS₂) thin films can be used as an efficient counter electrode (CE), an alternative to the conventional high cost Pt based CE. We are able to synthesis FeS₂ nanostructures utilizing a very cheap and easy hydrothermal growth route. MWCNT/TiO₂ mesoporous based DSSCs with FeS₂ CE achieved a high solar conversion efficiency of 7.27% under 100 mW cm⁻² (AM 1.5G 1-Sun) simulated solar irradiance which is considerably (slightly) higher than that of A-CNT/TiO₂ mesoporous based DSSCs with Pt CE. Outstanding performance of the FeS₂ CE makes it a very promising choice among the various CE materials used in the conventional DSSC and it is expected to be used more often to achieve higher photon-to-electron conversion efficiencies.

Dye-sensitized solar cells (DSSCs) have been intensively studied with a growing demand as potential alternatives for the next generation solar cells due to their low cost and eco-friendly production, easy processing, and relatively high energy conversion efficiency when compared with conventional solar cells^{1,2}. In contrast to the conventional solar cells, which relies on high purity substrates grown at very high temperatures using high cost processes in a specially designed environments such as clean room, DSSCs do not require such costly and complex processes and can be prepared in a simple laboratory environment without much concern on materials purity and ambient atmosphere³. A typical DSSC consists of TiO₂ mesoporous structures as photoanode deposited on fluorine doped tin oxide (FTO) coated glass substrate and sensitized by dye molecules and Pt coated FTO counter electrode (CE) with a I⁻/I₃⁻ redox electrolyte filled in between photoanode and CE⁴. Under solar irradiation, excited electrons in the Ruthenium-dyes are injected into the conduction band of TiO₂ nano-particles and diffuse into the FTO/TiO₂ interface and eventually are extracted to an external load⁵. The extracted electrons flow through the load and reach the CE. I⁻/I₃⁻ redox electrolyte accepts the electrons from Pt CE and those are transferred to the dye molecules to refill the holes in the HOMO⁶. Various methods are being investigated to increase the solar conversion efficiency of DSSCs⁷. Although the efficiency of the DSSCs has reached up to 11–12%, efforts to improve the photoelectron collection efficiency have been only reported in a few researches^{8,9}. The main problems in DSSCs are described as inefficient charge separation and electron transport, carrier recombination at surface states, cell instability, and inefficient adsorption of dye molecules on the FTO/TiO₂ surface^{10,11}. In recent years,

¹Department of Energy Systems Engineering, Faculty of Engineering, Yalova University, 77100, Yalova, Turkey.

²Department of Physics, Faculty of Science and Art, Erzincan University, Erzincan, 24100 Turkey. ³Department of Aeronautical Engineering, Istanbul Technical University, Maslak 34469, Istanbul, Turkey. ⁴Department of Chemical Metallurgical Engineering, Istanbul Technical University, Maslak 34469, Istanbul, Turkey. ⁵TUBITAK MAM Institute of Materials, Gebze, Kocaeli, 41400 Turkey. Correspondence and requests for materials should be addressed to B.K. (email: bkilic@yalova.edu.tr or kbayramkilic@gmail.com)

one dimensional (1D) nano-semiconductors with different morphologies such as nanorods, nanowires, nanotubes, nanobelts and nanosheets have been extensively used to improve the electron transport characteristic and to reduce the charge recombination in DSSCs^{12,13}, as well. Nanostructure based photoanodes grown by various type of materials in different nanostructure morphologies is another approach to increase the electron collection probability. Carbon based nanomaterials such as carbon nanotube and graphene can improve the overall performance of the cell through better electron transport properties caused by well-defined band alignment between adjacent layers^{14,15}. Carbon nanotubes (CNTs) with high electrical conductivity and very large surface area are an ideal substance for improving the charge transport and therefore the photo-generated current in photoanode of DSSCs^{16,17}. CNTs have been widely used in different layers of DSSCs such as in photoanode with the mixture of TiO₂, in counter electrode and solid state electrode for different applications¹⁸. However, it has been shown that the incorporation of CNTs in photoanode is the most effective way to improve the cell efficiencies due to better charge transport properties^{19,20}. MWCNT/TiO₂ photoanode based DSSC exhibits not only the advantage of high quality interface between CNTs and titania matrix, but also leads to the coexistence of dual pores which provide high surface area which is necessary for the dye adsorption^{10–21}. Besides photoanode components, CE also plays an important role to increase the solar conversion efficiency of DSSCs. In conventional DSSCs, Pt-coated FTO (Pt:FTO) and carbon are usually used as CE due to their exceptional catalytic activity, and high electrical conductivity²². Although DSSCs designed with Pt CE shows a good performance, Pt sources are scarce and increasing the cost of DSSCs²³. Carbon based CE, on the other hand, is cheaper than Pt, but it shows much lower performance when used as CE and therefore this drives the scientific community to look for other high performance and low cost materials to be utilized as CE in DSSCs²⁴. Recent works shows that FeS₂ nanostructures exhibit a high surface area which is beneficial for the catalytic reaction and the solar power conversion efficiency. FeS₂ with a optical energy band gap of 0.95–1.5 eV has attracted much interest with its inherent advantages such as excellent photo absorption, environmental compatibility, high electron mobility, large optical absorption coefficient, non-toxic and high quantum efficiency (>80%) in both fundamental research and practical applications^{25,26}. Since FeS₂ is thermodynamically stable in the corrosive I⁻/I₃⁻ redox liquid electrolyte this material has been extensively studied as possible alternative for Pt based CE in DSSCs²⁷.

In this paper, MWCNT/TiO₂ mesoporous photoanode is studied to investigate the effect of CNT based TiO₂ mesoporous on the DSSC performance and the enhancement capability of A-CNT/TiO₂ photoanode on solar conversion efficiency in DSSC is compared with a conventional TiO₂ photoanode. The Influence of MWCNT/TiO₂ photoanode on solar conversion efficiency of DSSC is compared with a conventional TiO₂ photoanode and result shows that efficiency is increased from 6.51% to 7.00% due to the enhanced light absorption and electron transport across the TiO₂ mesoporous based thin films. Besides photoanode components, we also demonstrate that FeS₂ nanostructures are very promising alternative ($\eta = 7.27\%$) to the Pt CE and it can be used as an efficient and low cost CE in DSSCs. Structural and optical characterizations are carried out using X-ray diffraction spectroscopy (XRD), scanning electron microscopy (SEM), energy dispersive spectroscopy (EDS), Raman spectroscopy and UV-Vis analyses.

Experimental

Preparation of A-CNT/TiO₂ Hybrid Photoanodes. Multiwalled CNTs (MWCNTs) were grown by thermal catalytic chemical vapor deposition (CVD) on silicon wafers using a thin catalyst layer of Fe/Al₂O₃ (1/10 nm) deposited by electron beam evaporation. MWCNT growth was performed in a quartz tube furnace (22 mm ID) at atmospheric pressure using ethylene as the carbon source. The nominal growth temperature was 750 °C, yielding an average growth rate (including nucleation and growth) of $\sim 2 \mu\text{ms}^{-1}$. Typically, CNT arrays are grown on 1 cm² Si wafers, resulting in well-aligned CNTs (MWCNTs) with densities of 10⁹–10¹⁰ CNTs cm⁻². As-grown CNT arrays have 1% volume fraction. The CNT arrays were kept face down in a vacuum chamber, facing the oxidizing agent (Details are described in our early work)²⁸. As-grown vertically-aligned multi-walled carbon nanotubes (MWCNTs) were dispersed onto a FTO (F:SnO₂) substrate (with a Sheet resistance of 14 Ω/sq) via contact printing. Aqueous solution of 1 mM titania (IV) oxide, 10 ml HCl and 40 ml deionized water were prepared and placed into a Teflon-lined stainless steel autoclave. 8 ml ammonia (28%) was added into the solution to adjust pH >4.5. MWCNT/FTO substrates were immersed into the solution and then heated to 175 °C for 24 hours. After hydrothermal growth processes, the whole system was allowed to cool down to the room temperature (RT) and substrate was blow dried by N₂. Finally, the TiO₂ mesoporous film was obtained on the MWCNT/FTO substrate and the sample were placed into a furnace at 450 °C for 40 min to minimize the defects.

Preparation of Iron Pyrite (FeS₂) Counter Electrodes. FeCl₃·6H₂O (Sigma-Aldrich) and Sulfur powder (%99.98) were used as precursor. 0.3 g iron chloride and 0.1 g sulfur were prepared in 40 ml DI water. The pH of the mixture was adjusted to 11 by adding a specific amount of Ammonia (%28). The solution was kept under magnetic stirring at RT for 1 h. The mixture was placed and sealed in a Teflon-lined stainless steel autoclave after immersing the FTO substrate into the solution. After that the autoclave was placed into an oven at 175 °C and kept there for 8 h to synthesis FeS₂ materials. A thin layer of FeS₂ nanostructures was obtained on the FTO substrate and washed with distilled water and ethanol several times to remove the excess of polymer and ion contaminants, and dried at 75 °C for 6 h in a vacuum oven. Finally, the film was sulfurized at 400 °C for 1 hr in nitrogen atmosphere.

Device Fabrication of DSSCs based on A-CNT/TiO₂ Hybrid Photoanodes and FeS₂ Counter Electrode. Hybrid DSSCs based on MWCNT/TiO₂ were prepared by adsorption of cis bis (isothiocyanato) bis(2,20-bipyridyl-4,40-dicarboxylato)-ruthenium(II)bis tetrabutylammonium (N719) dye onto the surfaces of the prepared photoanode for 6 h. It is important to note that the substrates were heated to 100 °C for 30 min before immersing into a 0.5 mM solution of the N719 dye. After 6 h the samples were taken out, rinsed with acetonitrile,

and dried with nitrogen gas. The dye-sensitized MWCNT/TiO₂ photoanode and FeS₂ counter electrode were sandwiched together using a 20 μm thick transparent Surlyn film (Meltonix 1170, Solaronix). The electrolyte, which consists of 0.5 M tetrabutylammonium iodide, 0.05 M I₂ and 0.5 M 4-tertbutylpyridine in acetonitrile, was injected between two electrodes and well distributed via capillary action. The active electrode area was typically 0.25 cm² for all type of cells studied in this work.

Characterization of the device. The structural and chemical characterizations of the nanostructures on each prepared sample were analyzed using Philips XL30 ESEM-FEG scanning electron microscope equipped with an EDAX energy dispersive X-ray spectroscopy detector. Crystal structure analysis was carried out using X-ray diffraction (XRD; Rigaku D/Max-IIIC diffractometer) with 1.54 Å Cu-Kα radiation and 2θ range of 20–80°. Absorption measurements were performed using a Perkin-Elmer UV-VIS Lambda 2S spectrometer. The Raman scattering measurements were performed using a micro Raman Renishaw 2000 system with an excitation source of 514.5 nm at RT. The infrared spectra were recorded using Fourier-transform infrared (FTIR) spectrometer, Perkin Elmer, in transmittance mode at 450–4000 cm⁻¹. Photocurrent density versus voltage (J-V) data were recorded using a Keithley 175A digital multimeter using a 0.01 V/s voltage ramp rate and an AM 1.5 solar simulator. The light source was a 250 W tungsten halogen lamp calibrated to irradiate the samples at 100 mW/cm² using a radiometer (IL1700, International). The incident photon current efficiency (IPCE) was measured with a spectral resolution of 5 nm using a 300W xenon lamp (Newport/Oriel). A reference scan of incident photon flux was taken using a calibrated Si photodiode.

Results and Discussion

The Effect of A-CNT Photoanodes on DSSC Performance. Top view and cross sectional SEM images of A-CNT/TiO₂ mesoporous photoanode are shown in Fig. 1(a,b) at different magnifications. ~1 μm long CNT arrays were coated with TiO₂ mesoporous structures and this is the key starting point of forming higher-phase hybrid system. Figure 1(b) shows that the FTO/MWCNT/TiO₂ hybrid system with inter-CNT spacing of 20–70 nm and it is clearly seen that CNT arrays were uniformly coated with TiO₂ without disturbing the CNTs' morphology. It is demonstrated that extremely high aspect ratio CNT arrays can be coated with TiO₂ mesoporous structures having about 30–50 nm pore radius. As seen in the SEM images, in the case of the TiO₂ coating the distance between the TiO₂ coatings 1% volume fraction CNTs have an average inter-CNT spacing of 70 nm, whereas TiO₂-coated CNTs have 40 nm of intertube spacing because of the 30 nm coating on each CNT. As seen in SEM images, the A-CNTs are well-dispersed within TiO₂ mesoporous thin film, and a good contact between nanotubes and TiO₂ mesoporous is achieved. This incorporation is very important for introducing an alternative electrical conduction pathway into the FTO/MWCNT/TiO₂ hybrid system. With high electrical conductivity of MWCNTs, it's expected to observe enhanced electron transport rate and life time in the TiO₂ mesoporous structure which eventually increase the solar conversion efficiency. The Raman spectroscopy measurements are carried out to further characterize the MWCNT/TiO₂ nanostructure complex. Raman scattering spectrum clearly identifies the phase of the TiO₂ mesoporous on the basis of its Raman band of Eg mode at 144 cm⁻¹. It is known that the Eg mode corresponds to O-Ti-O bending type vibration. Three peaks at 397, 515, and 638 cm⁻¹ in the Raman spectra of CNT/TiO₂ in Fig. 1(c) can be associated with the B1g (1), A1g+B1g (2), and Eg (2) modes of TiO₂, respectively. The other two peaks around 1340 and 1610 cm⁻¹ are associated with the characteristic D-band and G-band of CNTs corresponding to the disordered mode and tangential mode, respectively. Chemical characterization of the samples is carried out by Energy-dispersive X-ray spectroscopy (EDX). The EDX spectra of MWCNT/TiO₂ hybrid system is shown in Fig. 1(d) and shows the presence of major elements of C and O with strong Ti peaks. EDX quantitative analysis result of the MWCNT/TiO₂ hybrid film is presented in the inset of Fig. 1(d). In general, most of the MWCNT/TiO₂ hybrid film samples contain oxygen and titanium as major elements with small quantities of carbon.

XRD characterization is used to determine the crystallographic structure of the MWCNT/TiO₂ hybrid system. In Fig. 2(a,b), some well-defined diffraction peaks at 25.8°, 33.1°, 39.0°, 48.5°, 54.3°, 55.4°, 63.0°, 69.4°, 70.6°, and 75.4° can be observed. These peaks are assigned to the (1 0 1), (121), (231), (2 0 0), (1 0 5), (2 1 1), (2 0 4), (1 1 6), (2 2 0), and (2 1 5) reflections of crystalline anatase and brookite phase according to No. 21-1272 JCPDS, respectively. The result indicated that the main component of the thin film is anatase TiO₂. Among all diffraction peaks of MWCNT/TiO₂, (002) peak for CNT and (101) peak for TiO₂ mesoporous structures are thermodynamically the most stable due to the lowest surface energy. The peaks of 25.8°, 38.3°, 52.9° are associated with the typical peaks of CNT in (002), (100) and (004) directions, respectively. XRD characterization also shows brookite structures for TiO₂ mesoporous with CNT incorporation. Since carbon is very strong reducing agent, it would be likely to enhance the small transformation of anatase to brookite structures. The UV-Vis absorption spectra of the pure TiO₂ and MWCNT/TiO₂ nanostructures are shown in Fig. 2(c,d). As seen the MWCNT/TiO₂ exhibits a stronger visible light absorption than the pure TiO₂ mesoporous structures. The absorption edge of these also shifted towards the longer wavelength side, which indicates an ability of the hybrid systems to be photoactivated under the visible light irradiation. Furthermore, this may be referred to the mesoporous surface of the MWCNT/TiO₂ hybrid system and it is an advantage to absorb broader range of the solar spectrum. Figure 3(d) shows the (αhν)^{1/2} versus photon energy which was used to calculate the bandgap energy of MWCNT/TiO₂ and pure TiO₂ structures. The result indicates that the bandgap (Eg) of TiO₂ mesoporous is 3.15 eV, which is similar to the reported Eg (3.22 eV) value of TiO₂ and that of MWCNT/TiO₂ is 2.5 eV, which is slightly red-shifted. Modification of CNT with TiO₂ mesoporous not only increases the visible-light absorption but also provides a shift in absorption towards longer wavelengths.

The J-V characterization of the DSSCs based on nanostructured MWCNT/TiO₂ porous electrodes (under illumination of 100 mW cm⁻²) is shown in Fig. 3(a). The short-circuit photocurrent density (J_{sc}), open-circuit voltage (V_{oc}), fill factor (FF) and the corresponding energy conversion efficiency values (η) are summarized in

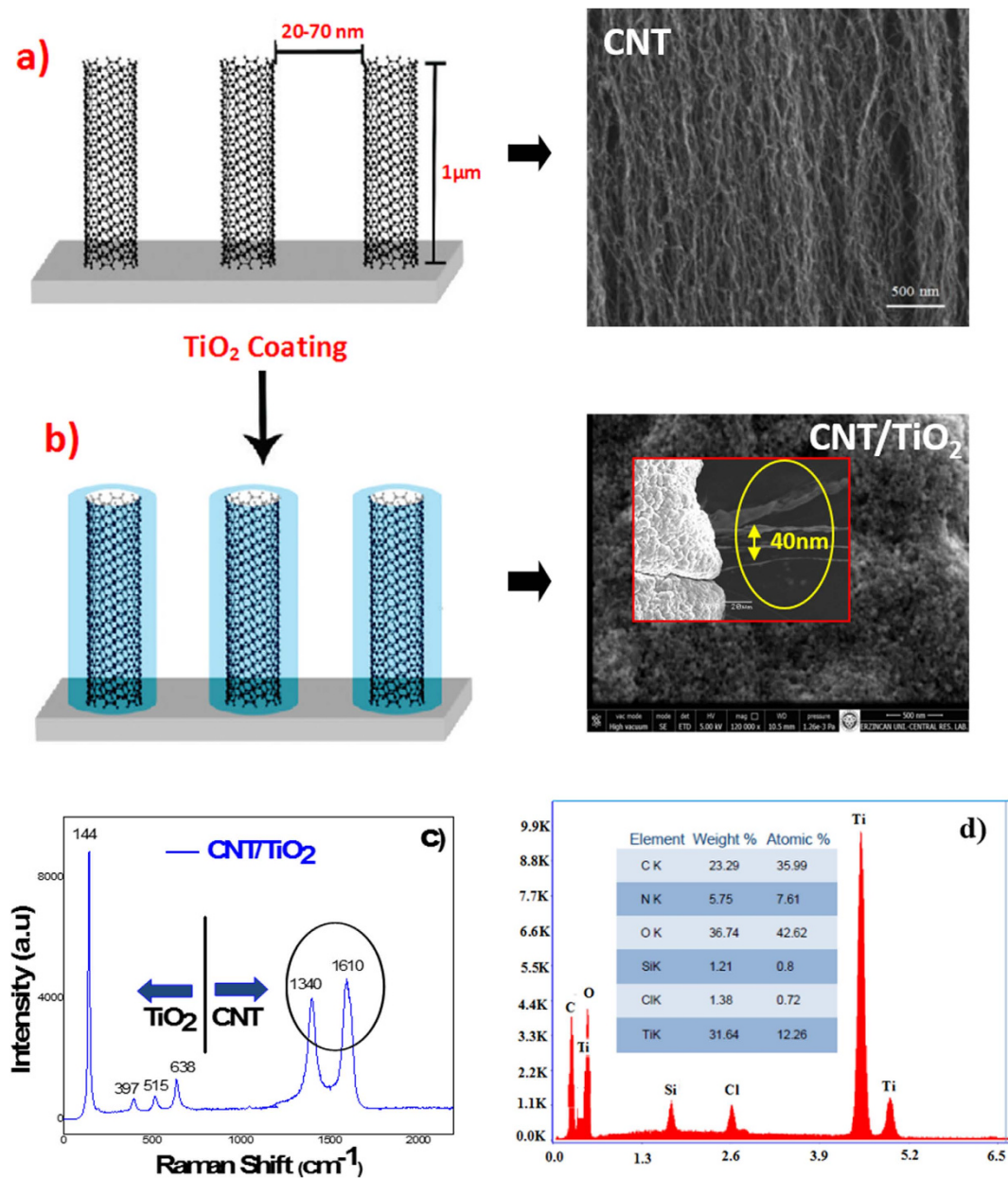


Figure 1. Top view and cross-sectional SEM images with corresponding schematic illustration of (a) CNT and (b) CNT/TiO₂ hybrid (network) structures (c) Raman and (d) EDAX spectra of CNT/TiO₂ complexes after annealing at 400 °C.

the inset table of Fig. 3. Compared with a DSSC based on conventional TiO₂ electrodes with Pt counter electrode, the MWCNT/TiO₂ layer containing 1 wt.% of CNTs provided an increase of device efficiency, which can be attributed to the enhanced J_{sc}. The DSSC with the hybrid photoanode and conventional Pt CE exhibited a short-circuit photocurrent (J_{sc}) of 15.96 mA cm⁻², open-circuit voltage (V_{oc}) of 0.77 V, FF of 57% and solar conversion efficiency (η) of 7.00%. For the DSSC with pure TiO₂ mesoporous photoanode and Pt CE fabricated using the same method, the values of J_{sc}, V_{oc}, FF and η were, 15.68 mA cm⁻², 0.77 V, 54% and 6.51%, respectively. The hybrid working electrode exhibits an enhanced photocurrent extraction compared with the pure TiO₂ electrode. The improvement on J_{sc} can be associated with an enhanced interconnectivity between CNTs and TiO₂ mesoporous structures. The CNT based photoanode introduces an alternative electrical conduction pathway that facilitates rapid electron transport in the photoelectrode. Nogueira *et al.* showed that the TiO₂-MWCNT photoanodes were prepared by a direct mixing method. They investigated that the performance of DSSC based on TiO₂-MWCNT photoanodes is dependent on the amount of MWCNT-COOH addition. When the amount of COOH content increased from 0 to 0.003 wt.%, solar conversion efficiency increased from 2.36% to 3.05²⁹. Lee *et al.* also introduced a similar behavior for the working electrode preparation with a small amount of 0.1 wt.% MWCNT³⁰. Ho *et al.* indicated that the DSSC with the TiO₂ photoanode containing 0.1 wt.% of MWCNT resulted in a higher current-density (J_{sc} = 9.08 mA cm⁻²) and a higher solar conversion efficiency (η = 5.02%)³¹. Park

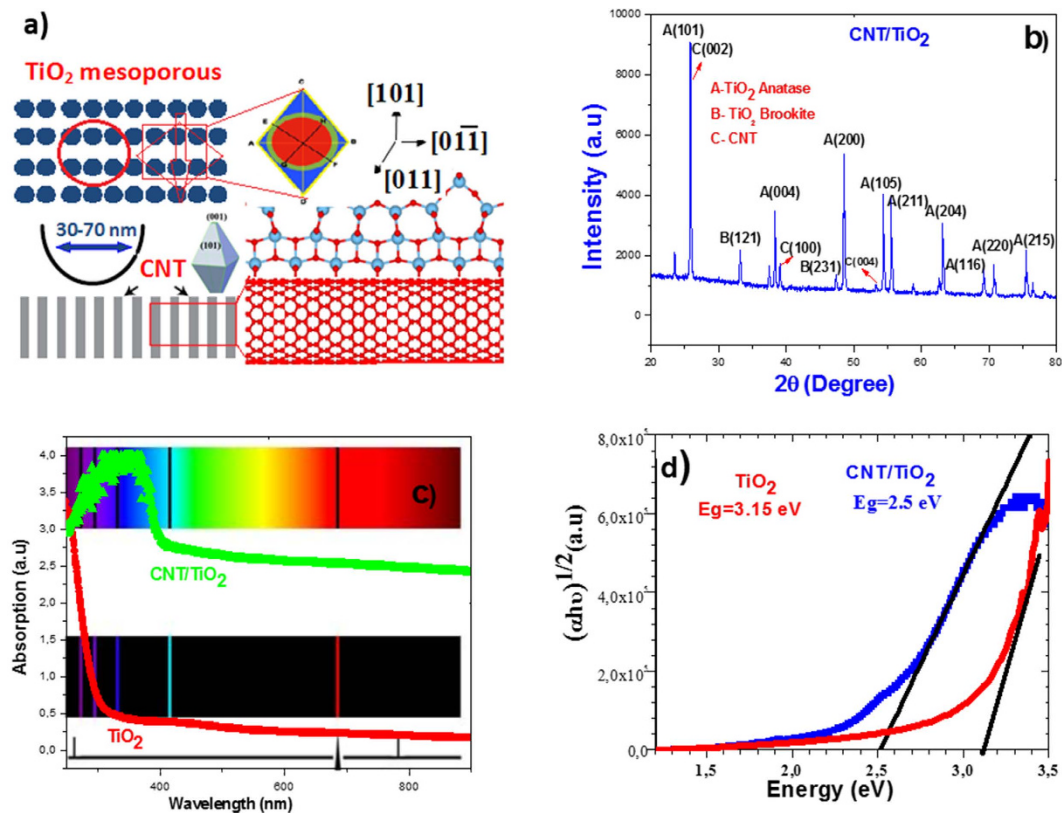


Figure 2. (a) Crystal structure and (b) XRD pattern of CNT/TiO₂ hybrid structures (c) Absorbance spectra and (d) Tauc plot of CNT/TiO₂ hybrid structures to determine the optical band gaps at room temperature.

et al. used the electro-spun carbon nanotubes/titanium dioxide (CNT/TiO₂) nanofibers fabricated using a mixture of titanium isopropoxide, MWCNT as photoanode material for DSSCs. DSSCs with CNT/TiO₂ nanofiber-based working electrodes with the addition of CNTs up to 5 wt.% increased the cell efficiency from 1.43% to 3.39%, while the further addition of CNTs resulted in a decrease of the cell efficiency³². Wang *et al.*³³ showed that the efficiency of DSSCs could be explained using LHE (light harvesting efficiency), electron injection efficiency, and electron collection efficiency, which relate to photo-current density. It was shown that the photo-generated electrons could recombine at the pure TiO₂/electrolyte interface due to a possible back diffusion of the carriers as illustrated in Fig. 3(d)³⁴. However, the use of CNTs in photoanode can quickly transport the photo-generated electrons and reduce the charge recombination probability. By adding an appropriate amount of CNTs to the working electrode, the electron transport characteristics are enhanced, and the collection time of electrons is decreased. As a result, faster collection of electrons results in a decrease in the rate of recombination leading the substantial enhancement in J_{sc} and solar conversion efficiency. To establish the benefit of the CNT/TiO₂ working electrodes, we investigated the incident photon-to-current conversion efficiency (IPCE) and electron transport properties of CNT/TiO₂ hybrid films. The observed improvement of IPCE can be explained by the increased light capture efficiency, electron injection and collection efficiency of the film. Figure 3(b) shows the IPCE spectra of the DSSCs with CNT/TiO₂ and pure TiO₂ photoelectrodes as a function of the wavelength. The IPCE at around 520 nm overlaps with the maximum absorption wavelength of the N719 dye. The device with a MWCNT/TiO₂ based electrode exhibits an enhancement of IPCE in the wavelength range of 350–600 nm, compared with that of the one with pure TiO₂ electrode. The enhancement of IPCE mainly resulted from the increased electron injection efficiency and LHE of the film. It is also attributed to the enhancement of dye loading via higher surface area of the hybrid film. Devices structure, photo-electrochemical reaction loop, and band alignment MWCNT/TiO₂ photoanode based DSSC with Pt CE are illustrated in Fig. 3(c,d). TiO₂ mesoporous structures accept electrons from photo-excited dye N719, and these electrons are transferred to the conduction band of CNTs through the transportation of electrons between TiO₂ mesoporous structures in a random and zigzag pathway. The electrons in the CNTs' conduction band, transferred from the TiO₂ conduction band, can quickly move to the FTO layer without any recombination or back reaction taking place. In contrast, pure TiO₂ based DSSC have a wide-band structure, hence electrons transferred from TiO₂ can stay at continuous energy levels near the Fermi level, accelerating recombination of electrons to the dye or back reaction to tri-iodide in the electrolyte.

Iron Pyrite (FeS₂) Thin Films for Counter Electrode in DSSC. FeS₂ thin films were prepared on a FTO coated glass substrate by a simple and cost effective hydrothermal method using (FeCl₃) 6H₂O and sulfur as precursor. The concentration of the sulfur precursor was intentionally kept higher to compensate the sulfur loss during the reaction. The thin film was annealed in a sulfur environment at 400 °C for 30 min to crystallize the film

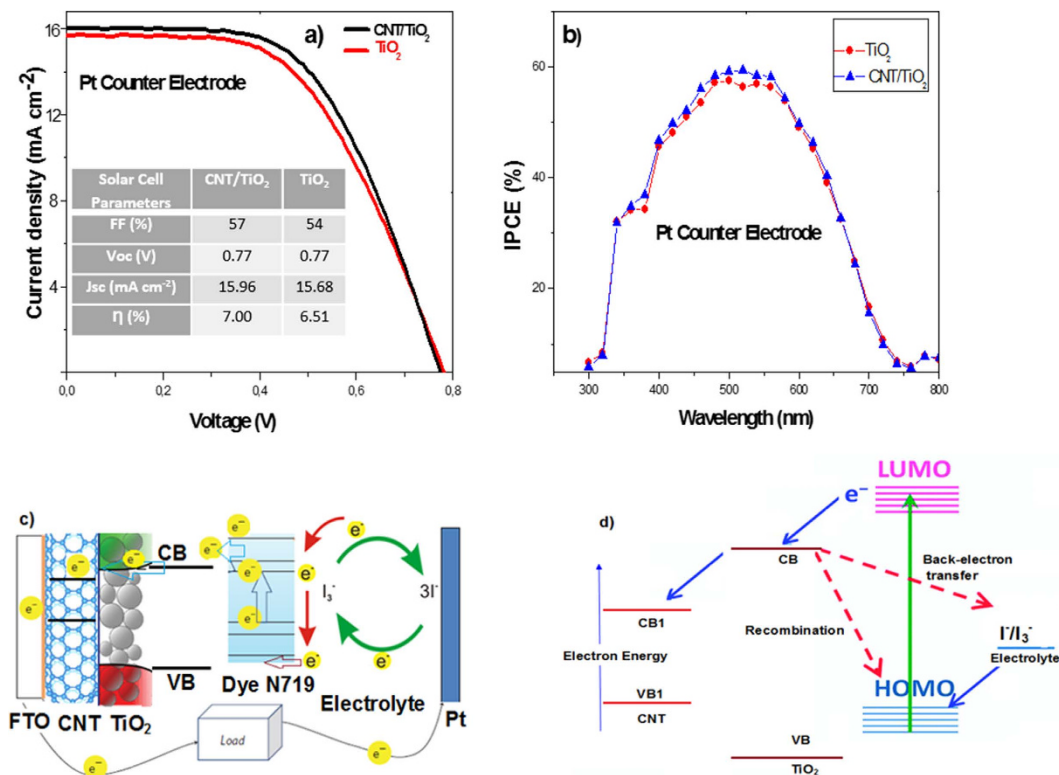


Figure 3. (a) Current density-voltage (J-V) characteristics of MWCNT/TiO₂ and TiO₂ photoanode with Pt CE based dye-sensitized solar cells under 1-Sun AM 1.5G solar irradiance (CNT wt% is 1 and the film thickness is about 15 μm) (b) IPCE spectra of the corresponding cells, (c) Schematic view of electron (e⁻) diffuse transport behavior in CNT/TiO₂-network hybrid electrode, (d) Energy level diagrams of the cell with possible loss mechanisms.

with appropriate stoichiometry. Figure 4 shows the SEM, EDAX, XRD, Raman, UV-Vis and surface photo-voltage results of FeS₂ thin film. The SEM images of FeS₂ thin film in Fig. 4(a) shows uniform and cubic shaped nanostructures after annealing. The effect of annealing temperature on the thin film can be attributed to the anisotropy of surface free energy and strain energy leading to huge growth during pyrite film formation. As seen in the SEM image, FeS₂ film contains large homogeneously distributed particles between 50–200 nm. The XRD diffraction peaks (Fig. 4a) can be indexed as a pure pyrite cubic phase of FeS₂ (JCPDS no 42-130), and no obvious impurity peaks were observed. The sharp peaks in the XRD pattern suggest the excellent crystallinity of the as-obtained FeS₂ thin film. The XRD peaks were recorded as (111), (200), (210), (211), (220), (311), (222), (023) and (321) at 2θ = 24.7, 33.6, 36.1, 41.3, 49.4, 54.3, 57.8, 62.4 and 64.3 degrees, respectively, which is indexed to FeS₂ cubic structure with high purity. The EDX analysis of the film shows the presence of Iron and sulfur in Fig. 4(b), and experiments showed that the iron concentration increases with temperature. The Fe:S ratio is approximately 33.3:66.6 at room temperature (figure not shown) and 50:30 at 400 °C. This result shows that the deposited FeS₂ thin film is transformed from FeS₂ to metallic Fe at 400 °C. The observed sulfur deficiency at elevated temperature is attributed to the low vapor pressure of Sulfur and therefore it sublimates easily at high temperatures. To investigate the chemical bonds and symmetry of molecules, the vibrational information was obtained from Raman spectroscopy. The Raman peaks confirm the phase purity of the film. The active Raman modes of the sample give a symmetric mode (A_g), doubly degenerate (E_g), and three triply degenerate modes. Figure 4(c) shows three Raman peaks at wave-numbers of 330, 370 and 435 cm⁻¹ that the characteristic active modes for FeS₂ are corresponding to the E_g and in phase stretching vibration of A_g, respectively. In the E_g mode, the S atoms are replaced vertically to the dimer axes. The peak at about 520 cm⁻¹ corresponds to the coupled vibration and stretching (T_g) modes or their combinations. As a result, the Raman peaks exhibit the FeS₂ cubic structure and further support the result gathered from XRD analysis. The optical properties of FeS₂ are investigated by UV-Vis spectroscopy. Figure 4(d) shows the absorption spectra of FeS₂ thin film. The FeS₂ film has a strong light absorption in the higher energy region. Figure 4(d) shows the graph of (αhν)^{1/2} vs. photon energy (hν) for FeS₂ thin film where the “α” is calculated from the absorption spectra utilizing the general formula for indirect allowed transition. The optical band gap energy value of FeS₂ thin film is obtained as 1.27 eV by fitting the rising portion of the curve in Fig. 4(d). UV-Vis results shows that the size of FeS₂ particles constituting the film can adjust the local structure and cause a strong change of optical properties. UV-Vis spectra indicated that the FeS₂ thin film with high density of grain boundaries can create strong photon scattering at interfaces and high optical absorption^{35,36}.

Figure 5(a) shows the current density-voltage performance of FeS₂ counter electrode DSSCs under 1-Sun illumination (100 mW/cm², AM 1.5G). The open-circuit voltage (V_{oc}), short-circuit current density (J_{sc}), and fill

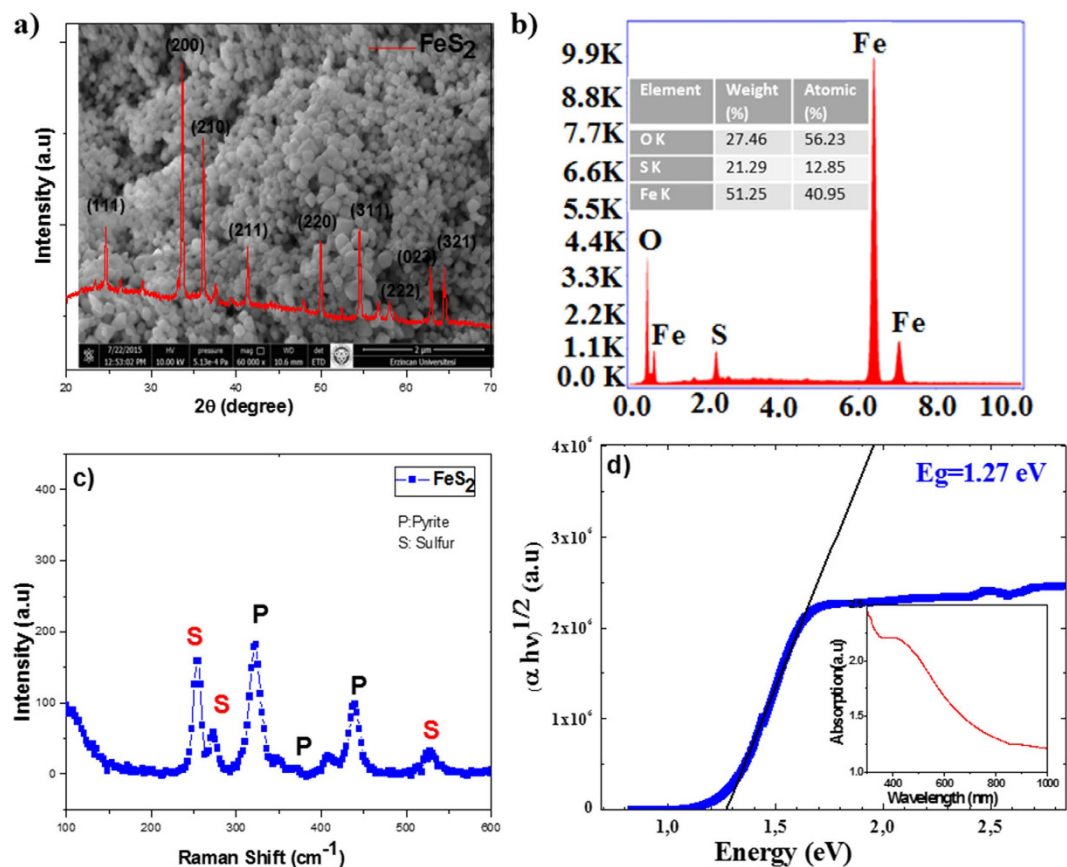


Figure 4. (a) XRD pattern of the FeS₂ particles with corresponding SEM image in inset. (b) EDAX analysis (c) Raman spectra (d) UV-Vis absorbance spectra of FeS₂.

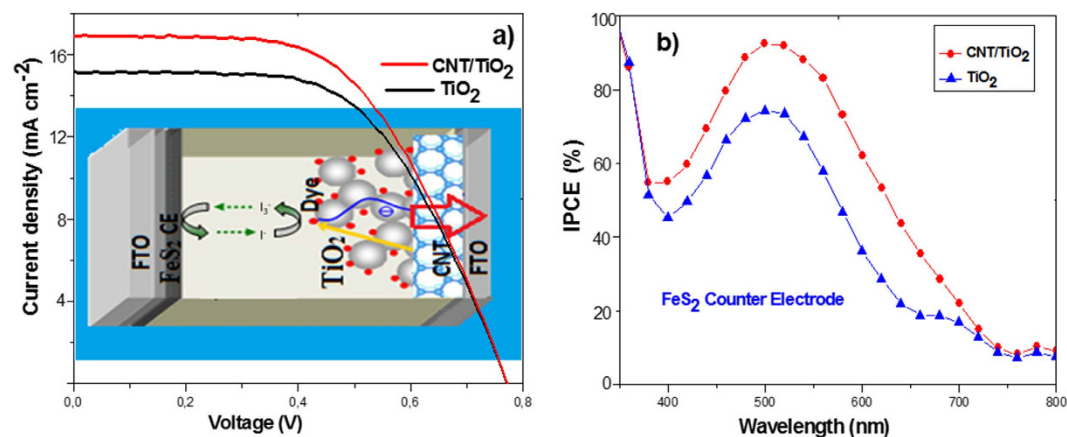


Figure 5. (a) Current density-voltage (J-V) characteristics of MWCNT/TiO₂ and TiO₂ WE DSSCs with FeS₂ thin films as CE. (FeS₂ film thickness is about 1 μm) Inset: Schematic diagram of a device with MWCNT/TiO₂ WE. J-V characteristics were obtained under 1-sun AM 1.5G solar irradiance, (b) IPCE spectra of the devices.

factor (FF) of MWCNT/TiO₂ photoanode based DSSC with FeS₂ CE are obtained as 0.77 V, 16.86 mA/cm², and 0.56, respectively, thus yielding an energy conversion efficiency of 7.27%. On the other hand, the corresponding values of the pure TiO₂ photoanode based DSSC with FeS₂ CE are measured 0.77 V, 15.16 mA/cm², 0.57 and 6.65%, respectively. The improvement of IPCE is mainly the consequence of increased J_{SC}, which can be attributed to rapid inter conversion between I₃⁻ and I⁻, possible reflection of incident photons from FeS₂ CE layer and appropriate bandgap energy of FeS₂. Since FeS₂ has a bandgap energy of 1.27 eV, photons can be absorbed in this layer and generated electrons in conduction band may contribute the J_{SC} of DSSC through the transport process either to electrolyte or TiO₂. It is shown that FeS₂ CE can also provide a large effective surface area owing to their rough morphology, leading to low charge transfer resistance. IPCE was found to shift upward in DSSCs when FeS₂

was used as CE in the place of conventional Pt material. IPCE spectra in Fig. 5(b) show typical characteristics of N719 dye at 520 nm. The upward shift of the IPCE curve is an indication of the extra electrons generated in the devices. The shift is consistent with the increment of the J_{sc} value apparently seen in Fig. 5(a). It has been clearly shown that FeS_2 materials have a good catalytic activity and have a big potential to be an ideal counter electrode for DSSC applications.

Conclusion

Multi-walled carbon nanotube (MWCNT) as working electrode on solar conversion efficiency in DSSC is being studied and MWCNT based working electrode showed a distinct improvement in photocurrent compared with the pure TiO_2 working electrode. The results show that the conversion efficiency of MWCNT/ TiO_2 based cell with conventional Pt CE was improved from 6.51% to 7.00% which is associated with the enhanced interconnectivity between CNT and TiO_2 mesoporous structures. In addition to the conventional Pt CE we designed a new CE with FeS_2 nanostructures contained thin film. It was shown that pyrite thin films exhibited higher surface area and good catalytic activity compared to the conventional Pt CE and therefore higher solar conversion efficiency of 7.27% was obtained from MWCNT/ TiO_2 hybrid photoanode based DSSC with FeS_2 CE. Based on the above results CNT based photoanode grown by a cheap and earth abundant material and catalytically more active FeS_2 CE grown by a simple and cheap hydrothermal method show a tremendous potential to be utilized in DSSCs industry to enhance the cell efficiency.

References

- Gratzel, M. Dye-sensitized solar cell. *J. Photochem. Photobiol. C* **4**, 145–153 (2003).
- Longo, C. & De Paoli, M.-A. Dye-sensitized solar cell: A successful combination of materials. *J. Braz. Chem. Soc.* **6**, 889–901 (2003).
- Poudel, P. & Qiao, Q. Carbon nanostructure counter electrodes for low cost and stable dye-sensitized solar cells. *Nano Energy* **4**, 157–175 (2014).
- Hagfeldt, A., Boschloo, G., Sun, L., Kloo, L. & Pettersson, H. Dye-sensitized solar cell. *Chem. Rev.* **110**, 6595–6663 (2010).
- Roy-Mayhew, J. D., Bozym, D. J., Punckt, C. & Aksay, I. A. Functionalized graphene as a catalytic counter electrode in dye-sensitized solar cells. *ACS Nano* **4**, 6203–6211 (2010).
- O'Regan, B. & Gratzel, M. A low-cost, high-efficiency solar cell based on dye-sensitized colloidal TiO_2 films. *Nature* **353**, 737–740 (1991).
- Dang, X. *et al.* Virus-templated self-assembled single-walled carbon nanotubes for highly efficient electron collection in photovoltaic devices. *Nature Nanotech.* **6**, 377–384 (2011).
- Yella, A. *et al.* Porphyrin-sensitized solar cells with cobalt (II/III)-based redox electrolyte exceed 12 percent efficiency. *Science* **334**, 629–634 (2011).
- Kılıç, B., Telli, H., Tüzemen, S., Başaran, A. & Pirge, G. Design of Hybrid Nanoheterostructure Systems for Enhanced Quantum and Solar Conversion Efficiencies in Dye-Sensitized Solar Cells. *J. App. Phys.* **117**, 135704 (2015).
- Golobostanfard, M. R. & Abdizadeh, H. Hierarchical porous titania/carbon nanotube nanocomposite photoanode synthesized by controlled phase separation for dye sensitized solar cell. *Sol. Ener. Mat. & Solar Cells* **120**, 295–302 (2014).
- Chung, I., Lee, B., He, J., Chang, R. P. H. & Kanatzidis, M. G. All-solid-state dye-sensitized solar cells with high efficiency. *Nature* **485**, 486–489 (2012).
- Feng, X. J. *et al.* Vertically aligned single crystal TiO_2 nanowire arrays grown directly on transparent conducting oxide coated glass: synthesis details and applications. *Nano Lett.* **8**, 3781–3786 (2008).
- Adachi, M., Murata, Y., Okada, I. & Yoshikawa, S. Formation of titania nanotubes and applications for dye-sensitized solar cell. *J. Electrochem. Soc.* **150**, G488–G493 (2003).
- Kongkanand, A., Domínguez, R. M. & Kamat, P. V. Single wall carbon nanotube scaffolds for photoelectrochemical solar cells. Capture and transport of photogenerated electrons. *Nano Lett.* **7**, 676–680 (2007).
- Wang, W., Serp, P., Kalck, P. & Faria, J. L. Photocatalytic degradation of phenol on MWNT and titania composite catalysts prepared by a modified sol-gel method. *App. Catalys. B: Environmental* **56**, 305–312 (2005).
- Fan, S. *et al.* Self-oriented regular arrays of carbon nanotubes and their field emission properties. *Science* **283**, 512–514 (1999).
- Tune, D. D., Flavel, B. S., Quinton, J. S., Ellis, A. V. & Shapter, J. G. Carbon Nanotube Network Electrodes for Dye Solar Cells. *Sol. Ener. Mat. & Solar Cells* **94**, 1665–1672 (2010).
- Golobostanfard, M. R. & Abdizadeh, H. Influence of carbon nanotube wall thickness on performance of dye sensitized solar cell with hierarchical porous photoanode. *Micropor. Mesopor. Mater.* **191**, 74–81 (2014).
- Lin, W.-J., Hsu, C.-T. & Tsai, Y.-C. Dye-sensitized solar cells based on multiwalled carbon nanotube–titania/titania bilayer structure photoelectrode. *J. Colloid Interface Sci.* **358**, 562–566 (2011).
- Dembele, K. T. *et al.* Effect of multi-walled carbon nanotubes on the stability of dye sensitized solar cells. *J. Power Sources* **233**, 93–97 (2013).
- Zhang, Q. & Cao, G. Hierarchically structured photoelectrodes for dye-sensitized solar cell. *J. Mater. Chem.* **21**, 6769–6774 (2011).
- Huang, S. *et al.* 3D hierarchical $FeSe_2$ microspheres: Controlled synthesis and applications in dye-sensitized solar cells. *Nano Energy* **15**, 205–215 (2015).
- Shukla, S. *et al.* Iron Pyrite Thin Film Counter Electrodes for Dye-Sensitized Solar Cells: High Efficiency for Iodine and Cobalt Redox Electrolyte Cells. *ACS Nano* **8**, 10597–10605 (2014).
- Ghamouss, F. *et al.* Characterization of screen printed carbon counter electrodes for Co(II)/(III) mediated photoelectrochemical cells. *Electrochim. Acta* **55**, 6517–6522 (2010).
- Xuefeng, Q., Yi, X. & Yitai, Q. Solventothermal synthesis and morphological control of nanocrystalline FeS_2 . *Mater. Lett.* **48**, 109–111 (2001).
- Ennaoui, A. *et al.* Iron disulfide for solar energy conversion. *Sol. Energy Mater. Sol. Cells* **29**, 289–370 (1993).
- Talapin, D. V., Lee, J.-S., Kovalenko, M. V. & Shevchenko, E. V. Prospects of Colloidal Nanocrystals for Electronic and Optoelectronic Applications. *Chem. Rev.* **110**, 389–458 (2010).
- Vaddiraju, S., Cebeci, H., Gleason, K. K. & Wardle, B. L. Hierarchical Multifunctional Composites by Conformally Coating Aligned Carbon Nanotube Arrays with Conducting Polymer. *ACS Appl. Mater. Interfaces* **1**(11), 2565–2572 (2009).
- Morais, A. *et al.* Enhancing in the performance of dye-sensitized solar cells by the incorporation of functionalized multi-walled carbon nanotubes into TiO_2 films: The role of MWCNT addition. *J. Photochem. Photobiology A: Chemist.* **251**, 78–84 (2013).
- Lee, T. Y., Alegaonkar, P. S. & Yoo, J. B. Fabrication of dye sensitized solar cell using TiO_2 coated carbon nanotubes. *Thin Solid Films* **515**, 5131–5135 (2007).
- Lee, K.-M., Hu, C.-W., Chen, H.-W. & Ho, K.-C. Incorporating carbon nanotube in a low-temperature fabrication process for dye-sensitized TiO_2 solar cells. *Sol. Energy Mater. Sol. Cells* **92**, 1628–1633 (2008).

32. Hieu, T. N., Baik, S. J., Chung, O. H. & Park, J. S. Fabrication and characterization of electrospun carbon nanotubes/titanium dioxide nanofibers used in anodes of dye-sensitized solar cells. *Synth. Met.* **193**, 125–131 (2014).
33. Wang, X., He, G., Fong, H. & Zhu, Z. Electron Transport and Recombination in Photoanode of Electrospun TiO₂ Nanotubes for Dye-Sensitized Solar Cells. *J. Phys. Chem. C* **117**, 1641–1646 (2013).
34. Hu, G. *et al.* Anatase TiO₂ nanoparticles/carbon nanotubes nanofibers: preparation, characterization and photocatalytic properties. *J. Mater. Sci.* **42**, 7162–7170 (2007).
35. Xia, J., Lu, X., Gao, W., Jiao, J., Feng, H. & Chen, L. Hydrothermal growth of Sn⁴⁺ doped FeS₂ cubes on FTO substrates and its photoelectrochemical properties. *Electrochim. Acta* **56**, 6932–6939 (2011).
36. Kılıç, B., Roehling, J. & Özmen, O. T. Synthesis and Optoelectronic Properties of Pyrite (FeS₂) Nanocrystals Thin Films for Photovoltaic Applications. *J. Nanoelectron. Optoelectron.* **8**, 260–266 (2013).

Acknowledgements

This project was supported by Türkiye Bilimsel ve Teknolojik Arastırma Kurumu (TÜBİTAK) (Scientific and Technological Research Council of Turkey). Project number: 114F292. The authors would like to thank TÜBİTAK for giving a generous support.

Author Contributions

B.K. had a design idea, initiated the research and supervised the overall project. S.T. analyzed all the data, evaluated the results and proof read the manuscript. A.A. prepared structural and optical characterization of TiO₂ mesoporous structures. O.C.O. prepared experimental section of FeS₂ thin films. M.A. prepared the figures of FeS₂ thin films. H.C. prepared MWCNT and wrote experimental section of MWCNT. D.U. prepared structural characterization of MWCNT. S.P.M. prepared J-V characterization of the cells. All authors were involved in the preparation of the manuscript.

Additional Information

Competing financial interests: The authors declare no competing financial interests.

How to cite this article: Kılıç, B. *et al.* Preparation of Carbon Nanotube/TiO₂ Mesoporous Hybrid Photoanode with Iron Pyrite (FeS₂) Thin Films Counter Electrodes for Dye-Sensitized Solar Cell. *Sci. Rep.* **6**, 27052; doi: 10.1038/srep27052 (2016).



This work is licensed under a Creative Commons Attribution 4.0 International License. The images or other third party material in this article are included in the article's Creative Commons license, unless indicated otherwise in the credit line; if the material is not included under the Creative Commons license, users will need to obtain permission from the license holder to reproduce the material. To view a copy of this license, visit <http://creativecommons.org/licenses/by/4.0/>